

# Synthesis of Ni,Co-doped MoS<sub>2</sub> as Electrocatalyst for Oxygen Evolution Reaction

Muhammad Sumair Sultan<sup>1</sup>, Waqar Uddin<sup>2,\*</sup>, Salma Hamza,<sup>1</sup> Abdullah K. Alanazi,<sup>3</sup>

<sup>1</sup> Department of Earth and Environmental Sciences, Bahria University, Karachi Campus

<sup>2</sup> Office of Research Innovation and Commercialization (ORIC), Bahria University, Karachi Campus

<sup>3</sup> Department of Chemistry, Faculty of Science, Taif University, P.O. Box 11099, Taif 21944, Saudi Arabia

\*E-mail: [vickyfuelche@yahoo.com](mailto:vickyfuelche@yahoo.com)

Received: 21 October 2022 / Accepted: 14 November 2022 / Published: 27 December 2022

Replacement of expensive state-of-art catalysts by cost-effective transition metal/composites is not only ease production of oxygen from water by electrochemical technique but also a step for the betterment of the green environment. In this regard, a composite of nickel and cobalt doped molybdenum disulfide (CoNiMoS<sub>2</sub>) electrochemical catalyst was synthesized by a hydrothermal method which was found efficient for oxygen evolution reaction (OER) in an alkaline medium with an overpotential of 1.477 mV at a current density of 1.0 mA.cm<sup>-2</sup>. Morphology of catalysts were analyzed through SEM & TEM. The brief explanation is that the pristine MoS<sub>2</sub> and NiMoS<sub>2</sub> were appeared flower-like petal nano-sheets whereas CoMoS<sub>2</sub> & CoNiMoS<sub>2</sub> seemed as a cubic structures. XRD & X-ray patterns has confirms crystallinity and composition of elements in composites. With the help of linear swept voltammetry (LSV) and electrochemical impedance spectroscopy (EIS), the polarization curves and charge transference resistance of catalysts were examined respectively.

**Keywords:** Green Environment; Electro-catalysis; Oxygen evolution reaction; Molybdenum disulfide; Doping; Over potential

## 1. INTRODUCTION

Humans consumed a lot of energy to fulfill their needs in daily life through transportation, industrial and commercial operations that mostly focused on fossil fuels i.e. oil, coal, and natural gas. It is the easiest and most convenient way to obtain energy sources but problems are associated with its scarcity and environmental hazards [1–6]. To overcome these shortcomings, alternate energy sources to fossil fuels are required. Most of the scientists believed hydrogen is an alternative source due to its huge abundance and is friendly to the environment when consumed. On a larger scale, hydrogen is produced by water splitting technique (electrochemical devices) in acidic/basic medium at cathode half-reaction

(hydrogen evolution reaction (HER)) while anode half-reaction (oxygen evolution reaction (OER)) hindered the efficiency of water-splitting due to slow chemical kinetics in an alkaline medium. In OER, 4-electron transfer processes switch various transitions of proton and electron, resulting in a huge overpotential and energy loss without a suitable catalyst [7,8]. Hence, minimal OER-overpotential is one of the main concerns to reduce the cost of H<sub>2</sub>- production in electrolysis [9–11]. Currently, commercial state-of-art catalysts such as RuO<sub>2</sub> and IrO<sub>2</sub> were generally used for OER performance in an alkaline medium which outstandingly decreases overpotentials but high cost and less availability on the earth's crust has reduce their applications on larger scale. Therefore, it is mandatory to explore the alternative cost-efficient and abundant electrochemical catalyst for water splitting [12,13].

Transition metal compounds such as phosphides [14][15], hydroxides [16], and sulfides [17] exhibit outstanding OER performance in basic solutions representing an alternative to noble catalysts especially the transition metal sulfides are more efficient among them due to their abundant active sites, good electric conductivity, and thermal stability. Catalytic activity is relay on compositions that why in reported literature the OER efficiency of transitions metals alloy is superior to a single metal compound i.e. the doping of single or multiple elements i.e. Cu, Co, Ni atoms, etc. into a single hybrid compound (sulfides) may increase their exotic and controllable properties [18–20].

In our current approach, a composite of double-doped (nickel and cobalt) molybdenum sulfate nanoparticles (CoNiMoS<sub>2</sub>) were synthesized by hydrothermal process for effective OER performance. Furthermore, the influence of doped elements in hybrid regarding conductivity, the extent of the active site, and the intrinsic of each site have also been analyzed.

## 2. EXPERIMENTAL SECTION

### 2.1. Reagents

All the analytical grade reagents i.e. ammonium molybdate tetrahydrate ((NH<sub>4</sub>)<sub>6</sub>Mo<sub>7</sub>O<sub>24</sub>·4H<sub>2</sub>O) (Shanghai Macklin Biochemical Co., Ltd), Nafion (5 wt. %), thioacetamide (CH<sub>3</sub>CSNH<sub>2</sub>) (Aladdin Industrial Corporation), nickel chloride (NiCl<sub>2</sub>) (Sinopharm Chemical Reagent Co., Ltd), Cobalt chloride (CoCl<sub>2</sub>) (Sinopharm Chemical Reagent Co., Ltd), NaOH (Aldrich), and ethanol (Sinopharm Chemical Reagent Co., Ltd) were commercially purchased and used without further purification.

### 2.2. Apparatus and Procedure

#### 2.2.1 Synthesis of Electrochemical Catalyst

The hydrothermal method was used to synthesize MoS<sub>2</sub> and its hybrid catalysts (NiMoS<sub>2</sub>, CoMoS<sub>2</sub> & CoNiMoS<sub>2</sub>). For CoNiMoS<sub>2</sub> preparation, 0.45g of (NH<sub>4</sub>)<sub>6</sub>Mo<sub>7</sub>O<sub>24</sub>·4H<sub>2</sub>O and 0.48 g of CH<sub>3</sub>CSNH<sub>2</sub> were uniformly dissolved in 30 ml distilled water and sonicated for about 40 minutes. 0.01g of nickel chloride and 0.01g of cobalt chloride were added to the mixture and further sonicated for 40 minutes. The mixture was then transferred into a 50ml Teflon autoclave and placed in an oven at 210°C

for 24 hours. The solution was allowed to cool at room temperature. Black residue was obtained through a centrifuge, and then washed several times with distilled water and ethanol. The residue was dried in the oven for 12 hours. Similarly, from the above-mentioned steps, single-doped MoS<sub>2</sub> (CoMoS<sub>2</sub> or NiMoS<sub>2</sub>) were prepared by 0.45g of (NH<sub>4</sub>)<sub>6</sub>Mo<sub>7</sub>O<sub>24</sub>•4H<sub>2</sub>O & 0.48 g of CH<sub>3</sub>CSNH<sub>2</sub> and 0.45g of (NH<sub>4</sub>)<sub>6</sub>Mo<sub>7</sub>O<sub>24</sub>•4H<sub>2</sub>O, 0.48 g of CH<sub>3</sub>CSNH<sub>2</sub> & 0.01g CoCl<sub>2</sub> or NiCl<sub>2</sub> precursors respectively. Whereas, pristine MoS<sub>2</sub> was prepared by mixing of 0.45g of (NH<sub>4</sub>)<sub>6</sub>Mo<sub>7</sub>O<sub>24</sub>•4H<sub>2</sub>O & 0.48 g of CH<sub>3</sub>CSNH<sub>2</sub> and 0.45g of (NH<sub>4</sub>)<sub>6</sub>Mo<sub>7</sub>O<sub>24</sub>•4H<sub>2</sub>O, 0.48 g of CH<sub>3</sub>CSNH<sub>2</sub> through above mentioned method.

### 2.2.2. Preparation of working electrode

The working electrode (glassy carbon) was first polished by continuous rubbing on alumina (Al<sub>2</sub>O<sub>3</sub>) for an hour and then 5 μL of homogenous slurry (a mixture of 1 ml of ethanol, 5 mg catalyst & 15 uL Nafion as a binding agent) of each sample was separately loaded on the working electrode and dried at room temperature. All voltammetry experiments were carried out by Electrochemical Base Station (CHI 660 E Shanghai Chen Hua). Polarization data (potential (1.0 V to 1.8 V) vs. SCE reference electrode) at a scan rate of 5 mV<sup>-1</sup> was obtained by putting the three electrodes i.e. working electrode, reference electrode (Ag/AgCl (in saturated KCl solution)), and counter electrode (carbon rod) into 1.0 M NaOH solution through linear sweep voltammetry (LSV) technique which was then calibrated for reversible hydrogen electrode (RHE).

Durability test and electrochemical double-layer capacitance surface area (ECSA) were measured through cyclic voltammetry at various scan rates with a narrow potential range while charge transference resistance of catalysts was examined by electrochemical impedance spectroscopy (EIS). Turn over frequency (TOFs) were calculated from the specific current density by using the following equation ( $A_{ECSA} = \text{Specific capacitance}/40\mu\text{F per cm}^2 \text{ per cm}_{ECSA}^2$  while  $\text{TOF} = (3.12 \times 10^{15} \text{ H}_2 \text{ s}^{-1} \text{ cm}^2 \text{ per mA cm}^{-2}) \times (j) / (1.42 \times 10^{15} \text{ atoms per cm}_{\text{real}}^2) \times A_{ECSA}$ ).

## 3. RESULT AND DISCUSSION

The structural morphology of MoS<sub>2</sub> and its composite catalysts were studied through scanning electron microscopy (SEM), transmission electron microscopy (TEM), and high-resolution transmission electron microscopy (HRTEM) as shown in Figure 1. According to SEM insight, MoS<sub>2</sub> & NiMoS<sub>2</sub> seemed to aggregate masses showing their uniform dispersion as indicated in (Figures 1a & 1c) respectively. CoMoS<sub>2</sub> appeared as cubic shaped (Figure 1e), whereas, the NiCoMoS<sub>2</sub> (Figure 1g) comprises a large number of cubic patterns along with aggregated mass (MoS<sub>2</sub>). Although, the presence of Ni couldn't be found in nickel-based composites NiMoS<sub>2</sub> & NiCoMoS<sub>2</sub> because a very trace amount of Ni was used in precursors. However, its presence can be detected by the X-ray diffraction technique (XRD) and X-ray photoelectron spectroscopy (XPS). TEM images for MoS<sub>2</sub> (Figure 1b) and NiMoS<sub>2</sub> (Figure 1d) are shown as flower-like petal nano-sheets with random orientations. Whereas, TEM insight of CoMoS<sub>2</sub> and NiCoMoS<sub>2</sub> illustrate cubic structure as seems in (Figures 1f & 1h) respectively. HRTEM

image of  $\text{CoNiMoS}_2$  has illustrated the interlayer space is about 0.63 nm (Figure 1i) which can be allocated to the diffraction plane of (002) of  $\text{MoS}_2$  lattice confirming the presence of Co in  $\text{MoS}_2$  lattice.

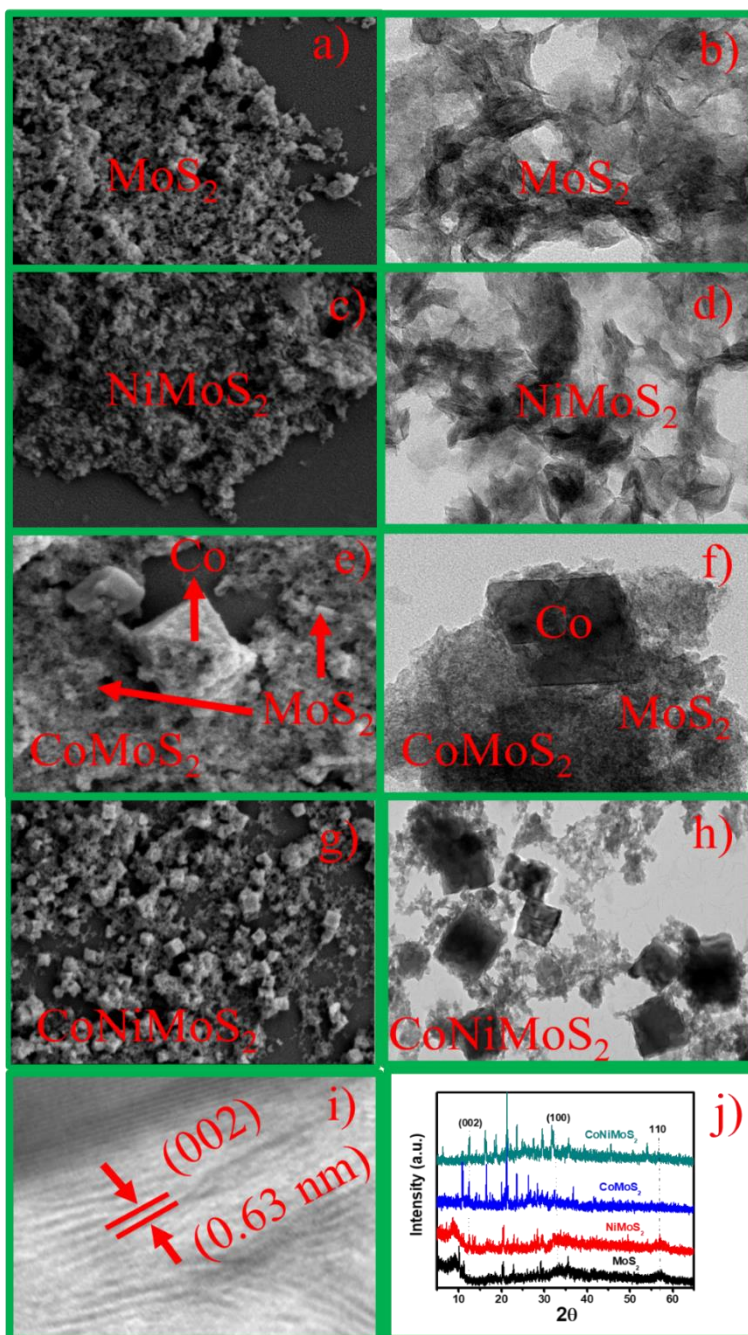


**Figure 1.** a) SEM of  $\text{MoS}_2$ ; b) TEM of  $\text{MoS}_2$ ; c) SEM of  $\text{NiMoS}_2$ ; d) TEM of  $\text{NiMoS}_2$ ; e) SEM of  $\text{CoMoS}_2$ ; f) TEM of  $\text{CoMoS}_2$ ; g) SEM of  $\text{CoNiMoS}_2$ ; h) TEM of  $\text{CoNiMoS}_2$ ; i) HRTEM of  $\text{CoNiMoS}_2$ ; j) XRD pattern of composite catalysts.

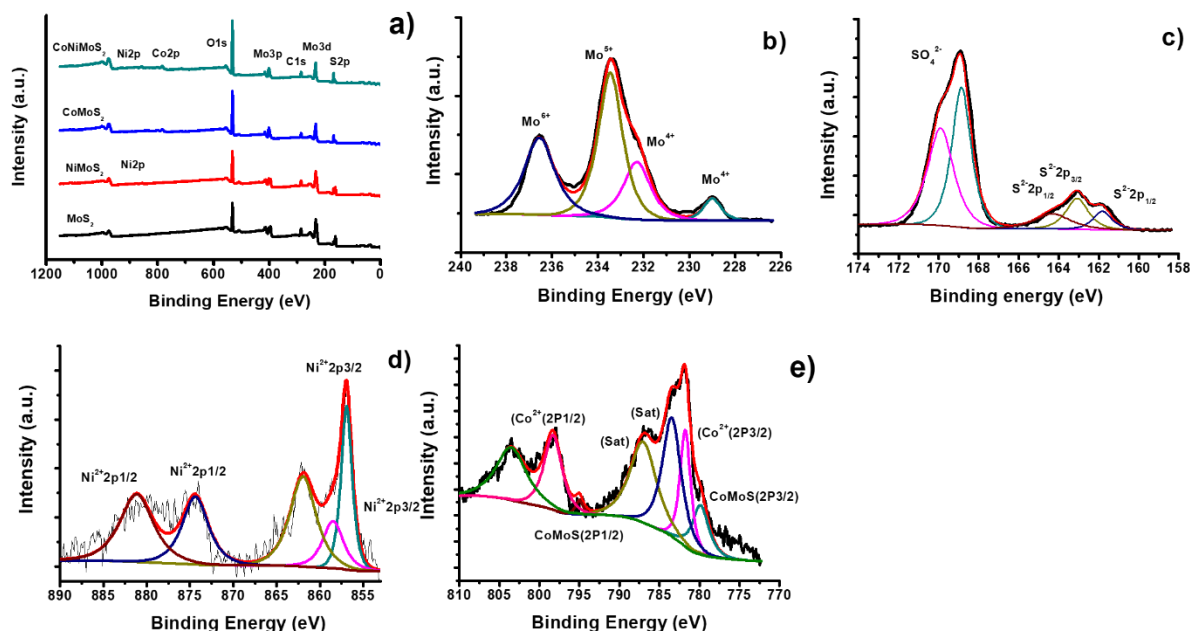


**Figure 2.** (a) XPS survey (b) Mo 3d (c) S 2p (d) Ni 2p (e) Co 2p for CoNiMoS<sub>2</sub>.

XRD pattern shows (Figure 1j) the crystalline structures of CoNiMoS<sub>2</sub>, CoMoS<sub>2</sub>, NiMoS<sub>2</sub> with slight diffraction at 13.8°, 32.2°, and 57.6° corresponding to the (002), (100), and (110) lattice plane of 2-H MoS<sub>2</sub> respectively (JCPDS 37-1492). Based on the d-spacing value of 0.63 nm (Figure 1i) and the primary peak lies at 13.8° of (002) of MoS<sub>2</sub> shows the incorporation of Co in MoS<sub>2</sub> structure [21,22]. Furthermore, the peaks that arise at 43° relate to the (200) planes of nickel [23].

X-ray photoelectron spectroscopy (XPS) survey via Figure 2a confirmed the existence of elements (Co, Ni, Mo & S) in pristine MoS<sub>2</sub> & composite catalysts. For better insight, High-resolution XPS of high-performer catalyst (CoNiMoS<sub>2</sub>) was analyzed as seen in Figure 2(b-e). Mo 3d insight (Figure 2b) shown two peaks at 229.4 eV and 232.2 eV revealing the +4 oxidation state of Mo (Mo3d<sub>5/2</sub> & Mo3d<sub>3/2</sub>) signifying 2H phase of MoS<sub>2</sub> [24,25]. The peak appears at 234 eV related to the Mo3d<sub>3/2</sub> of Mo<sup>5+</sup> indicating the IT phase of MoS<sub>2</sub> [26]. Similarly, a singlet peak at 137 eV attributed to the Mo<sup>6+</sup> indicates the presence of the oxide phase of Mo (Mo-O) [27][29]. S2p spectrum (Figure 2c), indicating three characteristic peaks at 161eV, 163 eV, and 164 eV attributed to S<sup>2-</sup> while two peaks 168 eV & 169.5 eV verify the S-O bond demonstrating the exposure of MoS<sub>2</sub> surface in air. Figure 2d indicated the Ni 2p spectrum, in which the peaks at 856.8 eV, 858.4 eV, 861.9 eV, 874.3 eV, and 881.4 eV confirmed the existence of Ni<sup>2+</sup>. Likewise, Figure 2e illustrates the Co 2p spectrum. Peak lies at 779.9 eV & 794.8 eV signify CoMoS 2p<sub>3/2</sub> & CoMoS 2p<sub>1/2</sub> phases respectively [28–30]. Two doublets at 781.7 eV & 798.3 eV represent 2p<sub>3/2</sub> & 2p<sub>1/2</sub> phase of Co<sup>2+</sup> [31,32] respectively. Whereas, two satellite peaks at 783.4 eV & 787.2 eV regarding the main peak for Co 2p<sub>3/2</sub> & 2p<sub>1/2</sub> are also noticed.

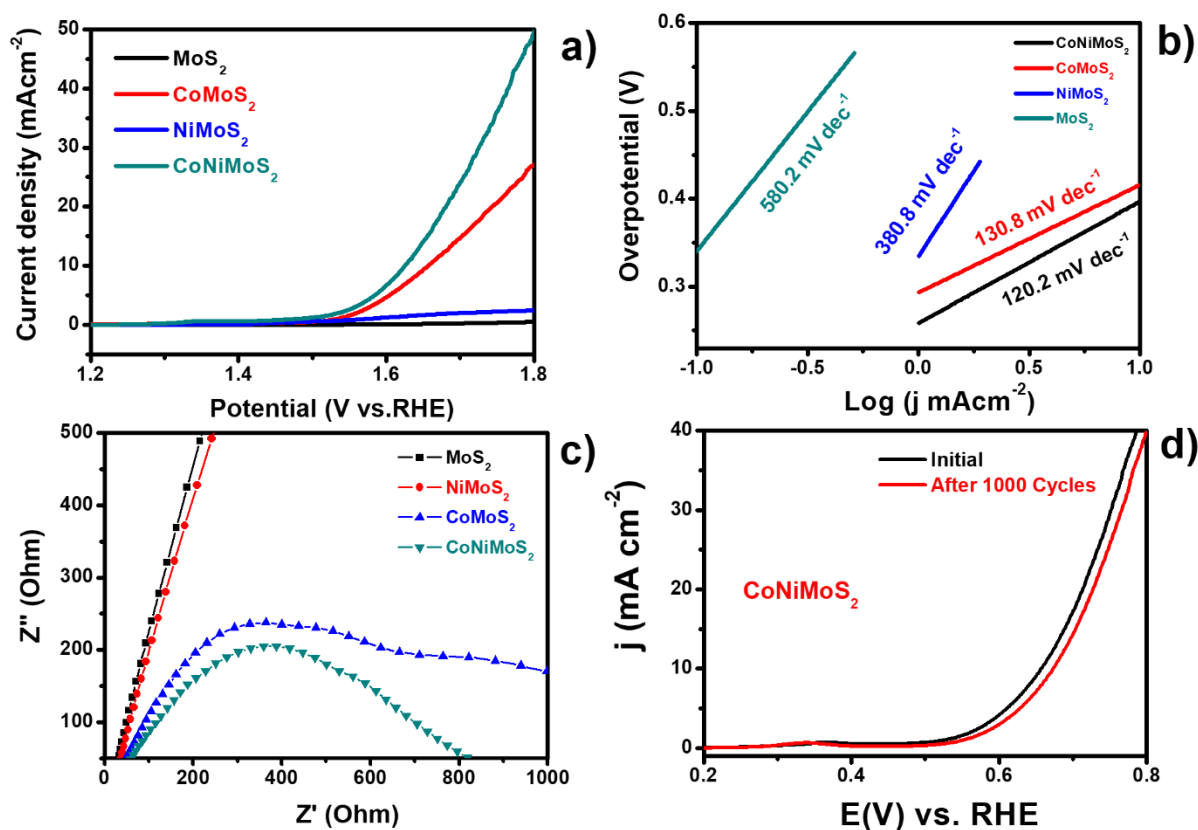


**Figure 3.** a) Polarization curves; b) Tafel plots; c) Nyquist plots; d) durability test of CoNi-MoS<sub>2</sub> in 1.0 M NaOH solution for OER.

OER performance of pristine MoS<sub>2</sub> and its composite catalysts (CoMoS<sub>2</sub>, NiMoS<sub>2</sub> & CoNiMoS<sub>2</sub>) was achieved with the help of a 3-electrode system in 1.0 M NaOH alkaline solution at room temperature. Experimental results indicated that the CoNiMoS<sub>2</sub> shows the best OER performance with a low overpotential of 1.477 mV as compared with CoMoS<sub>2</sub> (1.532 mV), NiMoS<sub>2</sub> (1.572 mV), & MoS<sub>2</sub> (1.8 mV) at a current density of 1.0 mA.cm<sup>-2</sup> (Figure 3a). The Tafel slope of each catalyst was calculated from their polarization curves just to know their kinetic rate of reaction, meaning that a smaller value of Tafel slope faster will be the OER reaction. Tafel slope in below ascending order of our prepared materials are obtained by putting polarization curve into Tafel equation ( $\eta = a + b \log j$ ), 120.2 mV dec<sup>-1</sup> CoNiMoS<sub>2</sub> > 130.8 mV dec<sup>-1</sup> CoMoS<sub>2</sub> > 380.8 mV dec<sup>-1</sup> NiMoS<sub>2</sub> > 580.2 mV dec<sup>-1</sup> MoS<sub>2</sub> as shown in the (Figure 3b). In contrast, CoNiMoS<sub>2</sub> has a lower Tafel slope showing promising OER performance. Furthermore, the obtained result has been compared with the published literature as well via Table 1. The stability of ternary composite was evaluated through cyclic voltammetric sweeps between 0.1 V to 0.5 V in 1.0 M NaOH solution for 1000 cycles as mentioned in (Figure 3c). We found after 1000 cycles that CoNiMoS<sub>2</sub> has good OER activity but shows little degradation.

**Table 1.** Comparison of Tafel Slope of CoNiMoS<sub>2</sub> with the Tafel Slope values of other reported materials.

Composites	Precursors	Tafel Slope mV dec <sup>-1</sup>	References
n-Co <sub>3</sub> O <sub>4</sub>	1M KOH	153	[33]
Co@TiO <sub>2</sub> /Ti	1M KOH	146	[34]
CoSi	50g/L H <sub>2</sub> SO <sub>4</sub>	428	[35]
NiFe	1M KOH	126.12	[36]
NiCo <sub>2</sub> O <sub>4</sub>	1M NaOH	132	[37]
NiS/NF	1M NaOH	140	[38]
Co <sub>2</sub> Mo <sub>3</sub> O <sub>8</sub> @NC	1M NaOH	126.65	[39]
CoNiMoS <sub>2</sub>	1M NaOH	120.2	This work

Charge transference resistivity of each catalyst was measured through electrochemical impedance spectroscopy (EIS) in ohm. As can be seen from the (Figure 3d), CoNiMoS<sub>2</sub> shows the least charge transference resistance ( $R_{CT}$ ) of 353  $\Omega$  as compared to CoMoS<sub>2</sub> = 368  $\Omega$ , NiMoS<sub>2</sub> = 4477  $\Omega$  and MoS<sub>2</sub> = 13606  $\Omega$ .

To investigate active site numbers of catalysts and to estimate turnover frequency (TOF), electrochemical capacitance surface area measurements were conducted. Electrochemical double layer charges for all these synthetic materials were obtained between potential swept of 200 to 500 mV vs. RHE 12 times for MoS<sub>2</sub>, NiMoS<sub>2</sub>, CoMoS<sub>2</sub>, and CoNiMoS<sub>2</sub> for six various scan rates (20 mV/S, 40 mV/S, 60 mV/S, 80 mV/S, 100 mV/S, 120 mV/S) as shown in Figure 4(a-d). The CoNiMoS<sub>2</sub> shows a higher capacitive current than the rest of the three catalysts at a scan rate of 80 mV S<sup>-1</sup> as shown in (Figure 4e). In addition to this, the calculated capacitive currents were plotted as a function of scan rate at 350 mV vs. RHE which determines more active sites for CoNiMoS<sub>2</sub> than NiMoS<sub>2</sub>, CoMoS<sub>2</sub>, and MoS<sub>2</sub> as shown in (Figure. 4f). Moreover, TOF values of MoS<sub>2</sub>, NiMoS<sub>2</sub>, CoMoS<sub>2</sub>, and CoNiMoS<sub>2</sub> were measured to be 2.8, 3.8, 4.4 and 7.5 H<sub>2</sub> S<sup>-1</sup> accordingly at 350 mV overpotential, determining the greater intrinsic activity of CoNiMoS<sub>2</sub> of each active site as compared to MoS<sub>2</sub>, NiMoS<sub>2</sub>, and CoMoS<sub>2</sub> in alkaline medium.

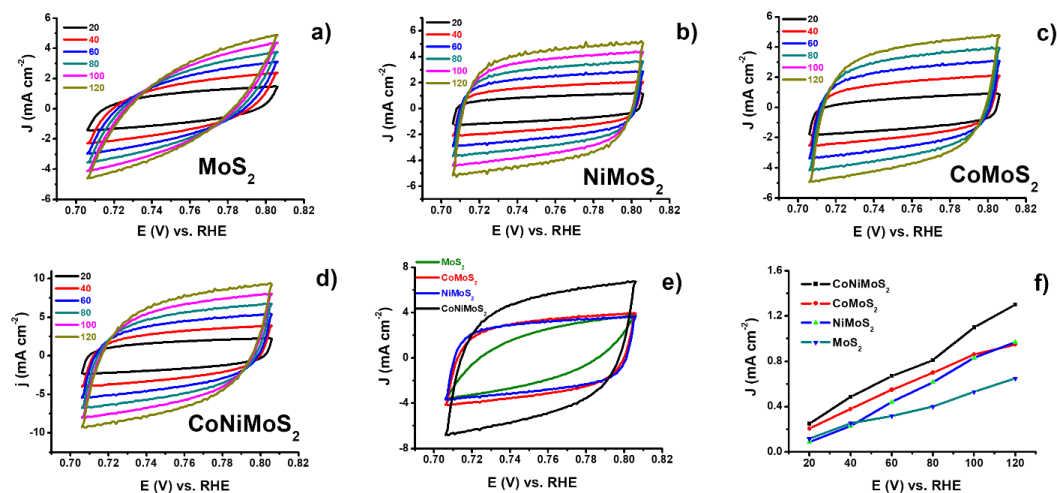


**Figure 4.** Electrochemical capacitance measurements: a). MoS<sub>2</sub>; b) NiMoS<sub>2</sub>; c) CoMoS<sub>2</sub>; d) CoNiMoS<sub>2</sub>; e) capacitive currents of MoS<sub>2</sub>, NiMoS<sub>2</sub>, CoMoS<sub>2</sub> and CoNiMoS<sub>2</sub> at 350 mVs<sup>-1</sup>; f) the capacitive current measured at 350 mV vs. RHE were designed as function of the scan rate for MoS<sub>2</sub>, NiMoS<sub>2</sub>, CoMoS<sub>2</sub> and CoNiMoS<sub>2</sub>.

#### 4. CONCLUSION

The double doped (Co & Ni) MoS<sub>2</sub> composite synthesized by the hydrothermal process is found a promising electrochemical catalyst for OER on lower overpotential (1.477 mV) at a current density of 1.0 mA.cm<sup>-2</sup>. The said ternary composite has a low Tafel value (120.2 mV dec<sup>-1</sup>), greater conductivity, durability & number of active sites.

#### ACKNOWLEDGEMENTS

The authors are gratefully acknowledged the support of Taif University Researchers (TURSP-2020/266).

#### References

1. I. Manisalidis, E. Stavropoulou, A. Stavropoulos, E. Bezirtzoglou, *Front. Public Heal.* (2020) 14.
2. J. Liu, J. Xu, Y. Chen, W. Sun, X. Zhou, J. Ke, *Int. J. Electrochem. Sci.*, 14 (2019) 359–370.
3. W. Yinwei, L. Shoufa, Z. Ning, Q. Xun, Z. Zhaofeng, *Int. J. Electrochem. Sci*, 14 (2019) 618–624.
4. S. Wang, W. Li, H. Qin, L. Liu, Y. Chen, D. Xiang, *Int J Electrochem Sci*, 14 (2019) 957–969.
5. X. Chen, B. Liu, C. Zhong, Z. Liu, J. Liu, L. Ma, Y. Deng, X. Han, T. Wu, W. Hu, *Adv. Energy Mater.*, 7 (2017) 1700779.
6. X. Fan, J. Liu, Z. Song, X. Han, Y. Deng, C. Zhong, W. Hu, *Nano Energy*, 56 (2019) 454–462.
7. K. Zhang, R. Zou, *Small*, 17 (2021) 2100129.
8. J. Song, C. Wei, Z.-F. Huang, C. Liu, L. Zeng, X. Wang, Z.J. Xu, *Chem. Soc. Rev.*, 49 (2020) 2196–2214.
9. B. Liu, S. Qu, Y. Kou, Z. Liu, X. Chen, Y. Wu, X. Han, Y. Deng, W. Hu, C. Zhong, *ACS Appl. Mater. Interfaces*, 10 (2018) 30433–30440.
10. S. Qu, Z. Song, J. Liu, Y. Li, Y. Kou, C. Ma, X. Han, Y. Deng, N. Zhao, W. Hu, *Nano Energy*, 39 (2017) 101–110.
11. Z. Wu, Z. Zou, J. Huang, F. Gao, *ACS Appl. Mater. Interfaces*, 10 (2018) 26283–26292.

12. B.T. Sneed, A.P. Young, D. Jalalpoor, M.C. Golden, S. Mao, Y. Jiang, Y. Wang, C.-K. Tsung, *ACS Nano*, 8 (2014) 7239–7250.
13. S. Zhang, Y. Hao, D. Su, V.V.T. Doan-Nguyen, Y. Wu, J. Li, S. Sun, C.B. Murray, *J. Am. Chem. Soc.*, 136 (2014) 15921–15924.
14. E. Hu, Y. Feng, J. Nai, D. Zhao, Y. Hu, X.W.D. Lou, *Energy Environ. Sci.*, 11 (2018) 872–880.
15. B. Song, K. Li, Y. Yin, T. Wu, L. Dang, M. Cabán-Acevedo, J. Han, T. Gao, X. Wang, Z. Zhang, *Acs Catal.*, 7 (2017) 8549–8557.
16. D. McAteer, I.J. Godwin, Z. Ling, A. Harvey, L. He, C.S. Boland, V. Vega-Mayoral, B. Szydłowska, A.A. Rovetta, C. Backes, *Adv. Energy Mater.*, 8 (2018) 1702965.
17. O. Mabayoje, A. Shoola, B.R. Wygant, C.B. Mullins, *ACS Energy Lett.*, 1 (2016) 195–201.
18. P. Kulkarni, S.K. Nataraj, R.G. Balakrishna, D.H. Nagaraju, M. V Reddy, *J. Mater. Chem. A*, 5 (2017) 22040–22094.
19. A.A. Yadav, Y.M. Hunge, S.-W. Kang, *Surfaces and Interfaces*, 23 (2021) 101020.
20. B.B. Kale, J. Baeg, S.M. Lee, H. Chang, S. Moon, C.W. Lee, *Adv. Funct. Mater.*, 16 (2006) 1349–1354.
21. S.-Q. Liu, K.-Z. Huang, W.-X. Liu, Z.-D. Meng, L. Luo, *New J. Chem.*, 44 (2020) 14291–14298.
22. J.-H. Lin, Y.-H. Tsao, M.-H. Wu, T.-M. Chou, Z.-H. Lin, J.M. Wu, *Nano Energy*, 31 (2017) 575–581.
23. K. Bhowmik, A. Mukherjee, M.K. Mishra, G. De, *Langmuir*, 30 (2014) 3209–3216.
24. M. Khan, A. Bin Yousaf, M. Chen, C. Wei, X. Wu, N. Huang, Z. Qi, L. Li, *Nano Res.*, 9 (2016) 837–848.
25. L. Wu, X. Xu, Y. Zhao, K. Zhang, Y. Sun, T. Wang, Y. Wang, W. Zhong, Y. Du, *Appl. Surf. Sci.*, 425 (2017) 470–477.
26. G. Eda, H. Yamaguchi, D. Voiry, T. Fujita, M. Chen, M. Chhowalla, *Nano Lett.*, 11 (2011) 5111–5116.
27. W. Park, J. Baik, T.-Y. Kim, K. Cho, W.-K. Hong, H.-J. Shin, T. Lee, *ACS Nano*, 8 (2014) 4961–4968.
28. J.E. Herrera, D.E. Resasco, *J. Catal.*, 221 (2004) 354–364.
29. C.P. Lienemann, S. Dreyfus, C. Pecheyran, O.F.X. Donard, *Oil Gas Sci. Technol. l'IFP*, 62 (2007) 69–77.
30. D. Laurenti, B. Phung-Ngoc, C. Roukoss, E. Devers, K. Marchand, L. Massin, L. Lemaitre, C. Legens, A.-A. Quoineaud, M. Vrinat, *J. Catal.*, 297 (2013) 165–175.
31. T. Wang, L. Wu, X. Xu, Y. Sun, Y. Wang, W. Zhong, Y. Du, *Sci. Rep.*, 7 (2017) 1–9.
32. G. Nasti, A. Abate, *Adv. Energy Mater.*, 10 (2020) 1902467.
33. C. Alex, S.C. Sarma, S.C. Peter, N.S. John, *ACS Appl. Energy Mater.*, 3 (2020) 5439–5447.
34. C. Yang, C.M. Makabu, X. Du, J. Li, D. Sun, G. Liu, *Electrochim. Acta*, 396 (2021) 139213.
35. B. Shen, Y. He, Z. He, Z. Wang, Y. Jiang, H. Gao, *J. Colloid Interface Sci.*, 605 (2022) 637–647.
36. X. YANG, Z. LI, Q.I.N. Jun, M. WU, J. LIU, G.U.O. Yong, F. Feng, *J. Fuel Chem. Technol.*, 49 (2021) 827–834.
37. H. Shi, G. Zhao, *J. Phys. Chem. C*, 118 (2014) 25939–25946.
38. Y.-W. Dong, B.-Y. Guo, Q.-W. Chen, B. Dong, *Int. J. Electrochem. Sci.*, 15 (2020) 5529–5539.
39. Y. Zhang, W. Ye, J. Fan, V. Cecen, P. Shi, Y. Min, Q. Xu, *ACS Sustain. Chem. Eng.*, 9 (2021) 11052–11061.